Advanced Composites and Hybrid Materials
https://doi.org/10.1007/s42114-017-0016-z

ORIGINAL RESEARCH

Surface morphology and beta-phase formation of single polyvinylidene fluoride (PVDF) composite nanofibers

Ehsan Ghafari[1] · Xiaodong Jiang[1] · Na Lu[1,2,3]

Received: 2 June 2017 / Revised: 26 June 2017 / Accepted: 6 July 2017

Abstract
This study has developed a reliable model to design and engineer PVDF nanofiber in terms of both morphological and fraction of beta-phase content based on response surface methodology (RSM). The model was further used to assess the effect of each individual electrospinning processing parameter as well as their interdependences on the properties of electrospun PVDF nanofibers. Our experimental results highly agreed with the modeling. The results indicated that both morphological and crystalline properties of PVDF are highly affected by electrospinning process parameters, particularly the fraction of beta-phase content. A beadless PVDF nanofiber with the maximum fraction of the beta phase was achieved through a numerical optimization process.

Keywords PVDF · Nanofiber · Bead-free · Electrospinning · Response surface method · Optimization

1 Introduction

Nowadays, energy harvesting is one of the most promising technologies due to concerns about the availability of non-renewable energy sources in the future [1–5]. Piezoelectric materials have been widely used as the primary element of many energy harvesters, to capture the energy from the vibration movements [6–9]. Poly (vinylidene fluoride) (PVDF) nanofibers have shown good ability to harvest the mechanical force under high strain conditions, due to their excellent flexibility and process simplicity [10]. PVDF has been widely investigated due to its piezoelectric and ferroelectric properties as well as its high flexibility, high durability, and good mechanical properties. The molecular structure of PVDF involves the repeated monomer unit $(-CH2CF2-)_{n.}$ PVDF is a semi crystalline polymer with the four distinctive crystal structures which can be divided into the polar and non-polar phases. Among them, three polar crystal forms exist (β, γ, and δ phases), where β-phase (TTTT) is highly polar compared to the other two phases. The non-polar α-phase (TGTG′), however, is the most common and thermodynamically stable phase at ambient temperature and pressure [11, 12]. The β-phase of PVDF is responsible for its electroactive properties such as ferroelectric, piezoelectric, and pyroelectric properties. The PVDF polymer chains in the unit cell of β-phase are arranged in a way that all the dipoles are aligned in a parallel manner leading to a net dipole moment, which is the strongest among all the phases [13–16]. Hence, the enhancement of beta phase of PVDF is essential for many applications.

Electrospinning is a widely used processing method to fabricate flexible PVDF nanofibers since it is simple, efficient, and cost effective. It has been reported that electrospun PVDF nanofiber results in the formation of the piezoelectric β-phase [17–20]. The electrospinning process involves applying a high electrical field and elongation force on nanofiber jet; it eliminates the need for post-treatment processes including electric poling and mechanical stretching. Despite electrospinning

✉ Na Lu
luna@purdue.edu

[1] Lyles School of Civil Engineering, Sustainable Materials and Renewable Technology (SMART) Laboratory, Purdue University, West Lafayette, IN, USA

[2] School of Materials Engineering, Purdue University, West Lafayette, IN, USA

[3] Birck Nanotechnology Center, Purdue University, West Lafayette, IN, USA

Published online: 27 November 2017

method appears to be technically straightforward, processing variables are not well understood and optimized in order to fabricate PVDF nanofibers with the desired properties [21]. For instance, the effects of each individual electrospinning process parameter on the properties of PVDF nanofiber have already been reported [18, 22–25]. The interdependences of each processing parameter on nanofiber characteristics have not been studied, since the conventional model only involves changing one of the electrospinning process parameters while keeping the others fixed at certain values. As results, the conventional methods do not provide a reliable model to predict and optimize the properties of PVDF nanofiber, and they are time-consuming and costly. Therefore, it is important to develop a comprehensive and reliable model to elucidate the effect of the electrospinning processing parameters on the morphology and the beta-phase formation of electrospun PVDF nanofiber. On the modeling part, the response surface methodology (RSM) has been approved as a powerful experimental design technique for the modeling and analysis of problems in which a response of interest is influenced by several variables [26–30]; however, the validity of using this method on PVDF nanofiber process has never been examined. To fill this knowledge gap, this paper aims to investigate the effect of electrospinning process parameters on the morphology and crystallinity of PVDF nanofiber. A RSM model is proposed to predict the size, the probability of the bead formation, and the fraction of beta-phase content of electrospun PVDF nanofiber. In addition, the proposed model was used to assess the effect of each electrospinning process parameter as well as the interdependences among all parameters. Finally, a multi-objective numerical optimization technique was used to achieve a bead-free PVDF nanofiber, simultaneous with the maximum of beta-phase content.

2 Experimental program

2.1 Materials and sample preparation

PVDF pellet (Mw = 275,000), N,N-dimethylformamide (DMF, Sigma 99.5%), and acetone (Sigma, 99.7%) were purchased from Sigma-Aldrich. In this study, PVDF solution was prepared by dissolving PVDF pellets in solvent mixtures of DMF/acetone. The solution was heated at 70 °C for 1 h followed by 5 h stirring at room temperature. The homogenous PVDF solution was then added to the 10-ml plastic syringe which was placed in a syringe pump. The positive voltage in range of 7.5 to 13.6 kV was applied to the needle to form Taylor cone (Table 1). The various feeding rate of the solution was adjusted to obtain a stable liquid jet. The nanofibers were spawned on a grounded rotating drum collector, which was placed at a distance of 10 cm from the tip of the needle.

Table 1 Variables and corresponding limits for fabrication of PVDF nanofiber

Symbols	Range of variation	
Variables	Min	Max
Concentration (%)	15	30
DMF/acetone (*v*/*v*)	0.2	3
Flow rate (ml/h)	0.5	3.8
Electrical field (kV/cm)	0.75	1.36

2.2 Development of RSM model

In this study, four independent processing variables, namely PVDF concentration, DMF/acetone ratio, flow rate, and electrical field, were studied. The variables defined for this experiment and their control levels are shown in Table 1. Three responses were considered, including nanofiber size, bead formation, and fraction of beta-phase content. It has to be noted that the addition of acetone above 83% caused clogging at the needle tip so that the electrospinning process was stopped. Therefore, the lowest DMF/acetone ratio was limited to 0.2.

2.3 Characterization of the samples

The diameter and morphology of the precursor and nanofiber were analyzed using scanning electron microscopy (SEM). Fourier transform infrared spectroscopy (FTIR) was performed to study different polymorphs of the samples and determine the fraction of beta phase of each electrospun PVDF sample.

3 Results and discussion

3.1 Model fitting and validation

A total of 33 set point combinations were randomly chosen according to D-optimal configuration for all four parameters. A second-order polynomial model was then calculated for each response. Establishing of the model was performed in three consecutive steps. First, a full polynomial model is applied to establish the relation between the electrospinning process and the responses. Second, the insignificant terms were removed from the model by conducting analysis of variance (ANOVA). The efficiency of the model was evaluated at the last step by performing residual analysis [26, 31, 32]. The adequacy of each proposed model was validated by coefficients of multiple determination (R^2), which implies the total deviation of the response variable from the predictive model [26, 28, 33]. The analyses of results for full regression models including the adjusted coefficient of multiple determinations

Table 2 Results for full regression models

Responses	Adj-R^2	Pre-R^2	F value	Lack of fit	Model P value
Fiber size	0.95	0.89	21.1	0.32	< 0.0001
Bead formation	0.92	0.85	16.8	0.46	< 0.0001
Beta-phase content	0.94	0.90	88.7	0.23	< 0.0001

(Adj-R^2), the predicted coefficient of multiple determinations (Pre-R^2), the lack of fit, and the model P value are given in Table 2. The obtained correlation coefficients for fiber size, bead formation, and fraction of beta phase were $R^2 = 0.95$, $R^2 = 0.92$, and $R^2 = 0.94$, respectively. These high values of correlation coefficient validate the adequacy of the model used to navigate the design space. ANOVA analysis was also performed to further evaluate the significance of the model. The F values 21.1, 16.8, and 88.7 were obtained for fiber size, bead formation, and fraction of beta phase, respectively, indicating that the models are significant. There is only a 0.01% chance that such a large F value could occur due to noise.

The adequacy of the model was verified by performing a lack-of-fit test (Table 2). The desired result is an insignificant lack of fit, presented by a value greater than 0.05 [34]. All the P values obtained by ANOVA implied that the lack of fit is not significant compared to the reference.

3.2 Morphology of PVDF nanofiber

Parameters affecting on the morphology and crystallinity of PVDF nanofiber can be classified into two groups including solution properties and electrospinning process parameters. The PVDF nanofiber size and formation of the beads are the two main characteristics that need to be controlled during the electrospinning process. SEM was used for visual analysis of the PVDF nanofiber morphology. The diameter and size distribution of the fibers were analyzed using ImageJ software. Figures 1 and 2 shows the morphology of two electrospun PVDF nanofiber mesh with the same concentration (25%) and different DMF/acetone ratios. The average diameter of nanofiber in sample 1 and sample 2 was around 87 and 438 nm, respectively. The SEM images of other two samples with the same PVDF concentration (27.5%) are presented in Fig. 3. Figure 3a shows a beadless PVDF nanofiber while Fig. 3b exhibits a high number of beads at the same concentration. The concentration of PVDF was reported widely as the most significant factor to minimize the beads in PVDF nanofiber [18, 25]; however, the substantial difference in nanofiber size (Figs. 1 and 2) and bead formation (Fig. 3) for the samples with the same concentration of PVDF pellets implies other electrospinning processes have more effects on morphology of electrospun nanofiber. In order to better present the complex relations between the parameters and responses, several 3D interaction surface graphs along with the trace plots obtained from RSM model were used as presented in Figs. 4 and 8.

Once the model was validated, the effect of each parameter on the response was systematically investigated. The ANOVA analysis was used to assess the effect of individual parameters as well as the interaction of variables on responses. The effect of variation of concentration and DMF/acetone ratio on nanofiber size is shown in Fig. 4. The higher concentration resulted in higher solution viscosity and stronger intermolecular interactions which led to larger nanofiber size. However, the amount of acetone plays a critical role in controlling the fiber size. For a constant electrical field and flow rate, the higher DMF/acetone ratio led to a finer fiber size; as shown in Fig. 2, higher acetone content increases the evaporation rate. In order to have a better understanding of each individual constituent

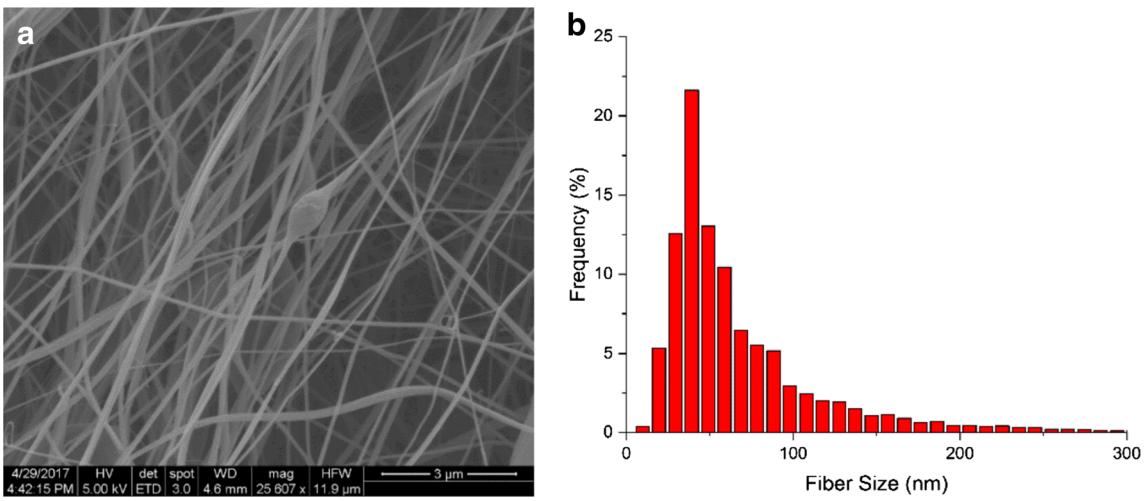

Fig. 1 PVDF nanofibers at concentration of 25%, DMF/acetone—3; **a** SEM image. **b** Fiber size distribution

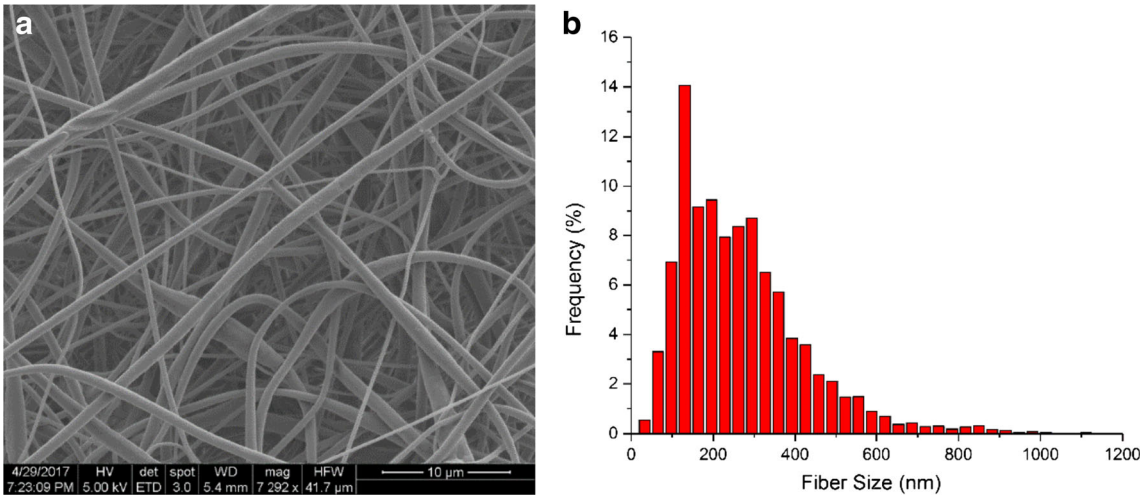

Fig. 2 PVDF nanofibers at concentration of 25%, DMF/acetone—1; **a** SEM image. **b** Fiber size distribution

effect on the response, a trace plot was used. A constituent effect curve displays how a model predicts that the response will change as the constituent is decreased or increased from its level in the reference mixture [28]. Figure 5 shows the effect of variation of all constituents on PVDF nanofiber size. The slope of the plot indicates the sensitivity of the response in terms of each constituent. The results indicated that higher electrical field leads to the formation of the fine fibers. In fact, applying the higher voltage might impose a higher charge density on the surface of nanofiber jet. This induces a larger elongation force to the fiber jet which results in a finer nanofiber size. As it can be seen, flow rate curve showed almost a horizontal trend, which implies that the nanofiber size is not very sensitive to this parameter.

The formation of beads has been widely reported in the electrospinning process [35–37], and it has been considered as the main drawback of the electrospun fibers [35]. The formation of bead-free nanofibers is favorable in almost all applications of electrospun nanofibers. The formation of beads in electrospun nanofibers is mostly related to the instability of the jet of polymer solution [38, 39]. In this study, the amounts of beads in microstructure of the nanofiber were measured quantitatively using ImageJ software. Figure 6 shows the variation of the bead formation in PVDF nanofiber as functions of concentration and DMF/acetone ratio. The results indicated that the amounts of beads increase with the decrease of concentration. In general, the lower concentration increased the risk of bead formation in PVDF nanofiber. The low viscous solution favors the formation of beads in PVDF nanofiber due to lack of sufficient polymer entanglement [40]. The results indicated the number of beads was reduced drastically for the solution with the concentration above 25%. However, several

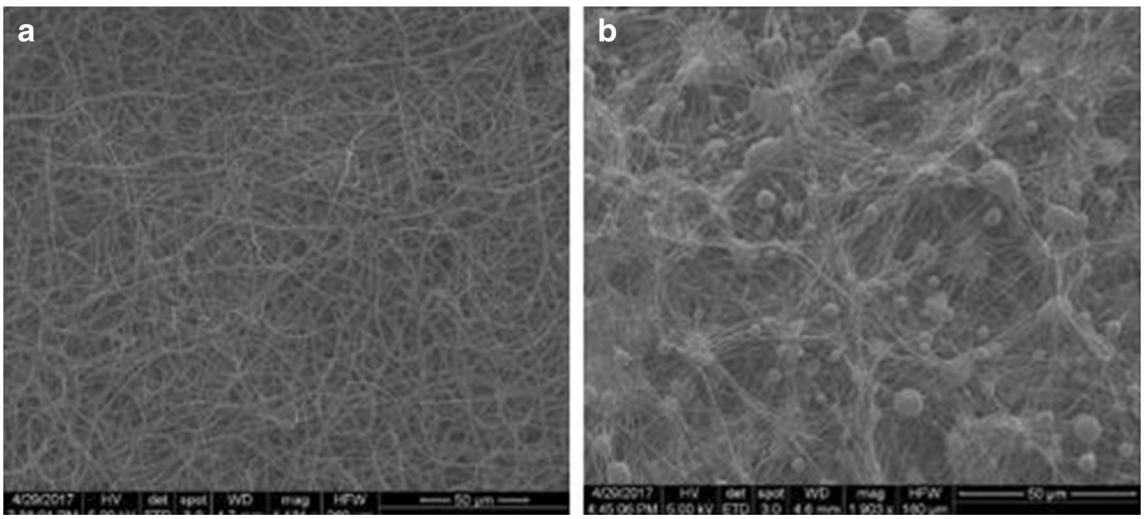

Fig. 3 Scanning electron microscopy image of nanofibers with concentration of 27.5%. **a** A beadless nanofiber. **b** PVDF nanofiber with a high number of beads

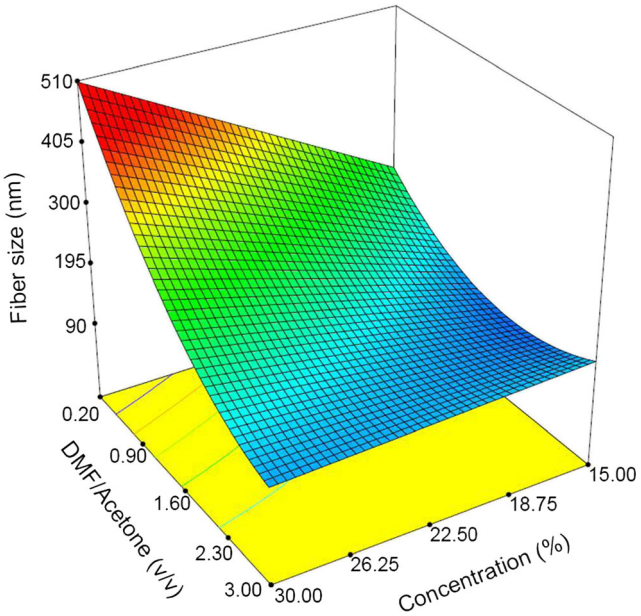

Fig. 4 3D fiber size plot as function of concentration and DMF/acetone

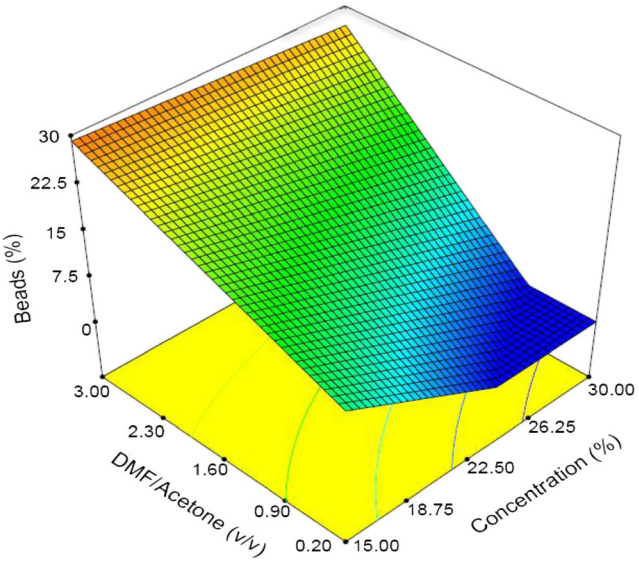

Fig. 6 3D bead formation plot as function of concentration and DMF/acetone

electrospun nanofiber samples with high concentration of PVDF pellets (more than 25%) exhibited considerable amount of beads, implying that the solution concentration itself does not necessarily result in a bead-free nanofiber. The DMF/acetone was to be found very effective in decreasing the amount of beads in PVDF nanofiber. However, the increase in DMF/acetone ratio results in nanofiber with increased beads may be attributed to the incomplete solvent evaporation. Indeed, the high volatility of acetone increased the evaporation rate of the solution which causes the jet to dry faster and thus impeding the electrospun jet breaking up into droplets [25]. Also, the addition of acetone reduces the surface tension of the solution so that beaded fibers can be converted into smooth fibers [41]. Hence, when the acetone concentration in the solution increased up to 60%, the number of beads reduced drastically, allowing to achieve a bead-free nanofiber at concentration even lower than 25%.

3.3 Beta-phase formation

The ferroelectric and piezoelectric properties of PVDF nanofiber are attributed to the fraction of β-phase. FTIR analysis is

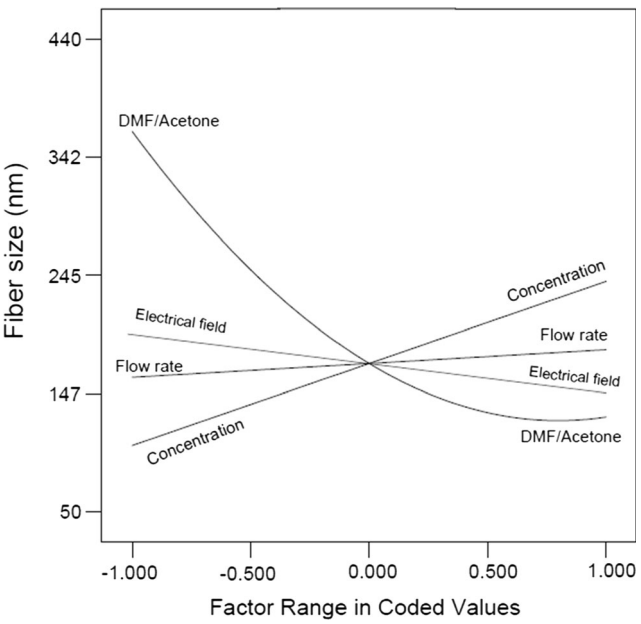

Fig. 5 Trace plot of PVDF nanofiber size

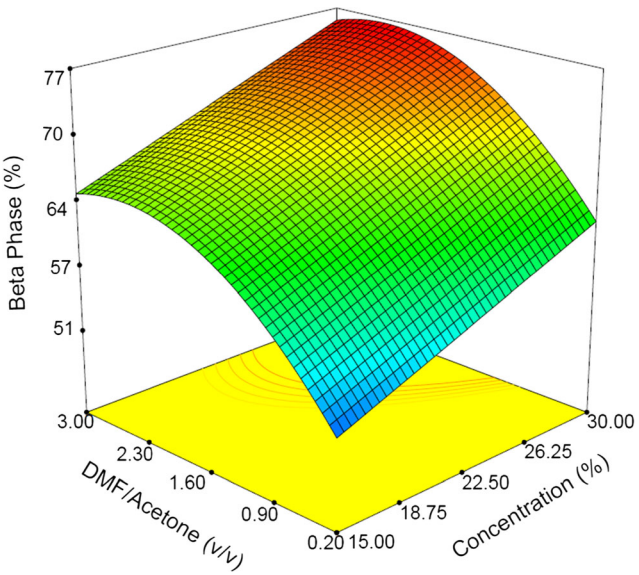

Fig. 7 3D fraction of beta phase plot as function of concentration and DMF/acetone

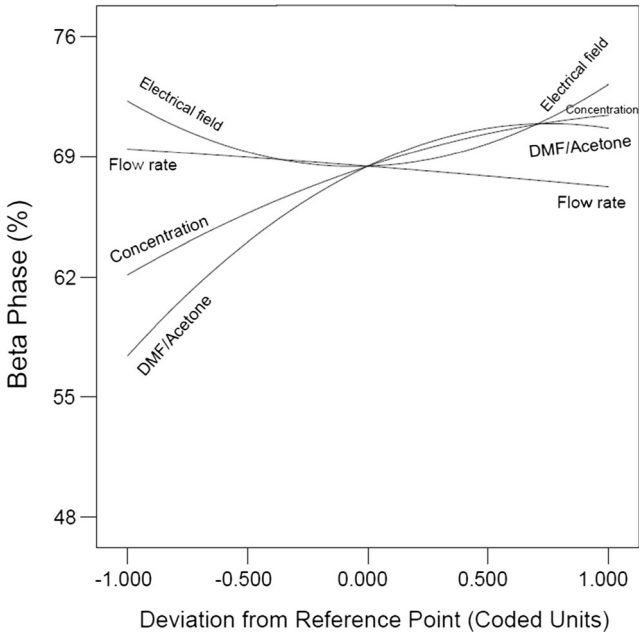

Fig. 8 Trace plot for fraction of beta phase in PVDF nanofiber

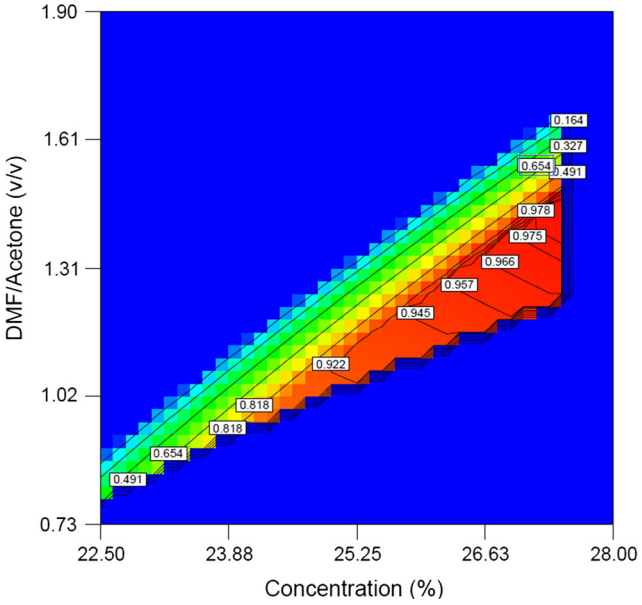

Fig. 9 Response surface plots of the Derringer's desirability function in correlation with a variation of concentration and DMF/acetone ratio

mostly used to quantify the electroactive phase content of PVDF. Assuming that FTIR absorption follows the Lambert-Beer law, the relative fraction of the β-phase in a sample containing just α and β PVDF is (Eq. 1) [42]:

$$F_\beta = \frac{A_\beta}{\left(K_\beta/K_\alpha\right)A_\alpha + A_\beta} \quad (1)$$

where $F(\beta)$ represents the phase content; A_α and A_β are the absorbance at 766 and 840 cm^{-1}; and K_α and K_β are the absorption coefficients at the respective wavenumber, which values are 6.1 × 104 and 7.7 × 104 cm^2 mol^{-1}, respectively.

The fraction of β-phase as function of concentration and DMF/acetone ratio is presented in Fig. 7. The results indicated that the fraction of β-phase is considerably decreased by reducing the DMF/acetone ratio. This might be due to the solvent evaporation rate which can be divided into three levels including low, intermediate, and high evaporation rates. It has been reported that low evaporation rates result mainly in the α-phase which are thermodynamically more favorable, while intermediate rates in a mixture of α and β and high evaporation rates in the α-phase are kinetically more favorable [43]. In fact, adding more acetone increases the evaporation rate of the solution, since it has a lower evaporation temperature, and this leads to the formation of more α-phase in PVDF nanofiber samples. The trace plot (Fig. 8) clearly confirms the significant effect of the acetone content on fraction of beta-phase content. As can be seen, the fraction of beta phase increased by increasing the concentration of PVDF pellets. High concentration of PVDF decreases the evaporation rate of the solution resulting in a formation of a high fraction beta-phase content. The simultaneous interaction effects of low concentration (15%) and high volume of acetone content (83%)

Table 3 Optimization of individual responses for a bead-free PVDF nanofiber with the highest fraction of beta phase

Responses and variables	Lower	Upper	Criteria	
			Goal	Importance
Concentration (%)	15	30	In range	5
DMF/acetone (*v*/*v*)	0.2	3	In range	5
Flow rate (ml/h)	0.5	3.8	In range	5
Electrical field (kV/cm)	0.75	1.36	In range	5
Fiber size (nm)	58	300	In range	5
Beads (%)	0.1	2	Minimize	5
Beta phase (%)	0.48	0.76	Maximize	5

Table 4 Optimum parameters for the proposed criteria

Constituents and responses		
	*M*1	*M*2
Concentration (%)	27.5	26
DMF/acetone (*v*/*v*)	1.49	1.25
Flow rate (ml/h)	2	1.5
Electrical field (kV/cm)	1.36	1.36
Fiber size (nm)	265	295
Beads (%)	0.09	0.09
Beta phase (%)	75	71
Desirability	0.98	0.96

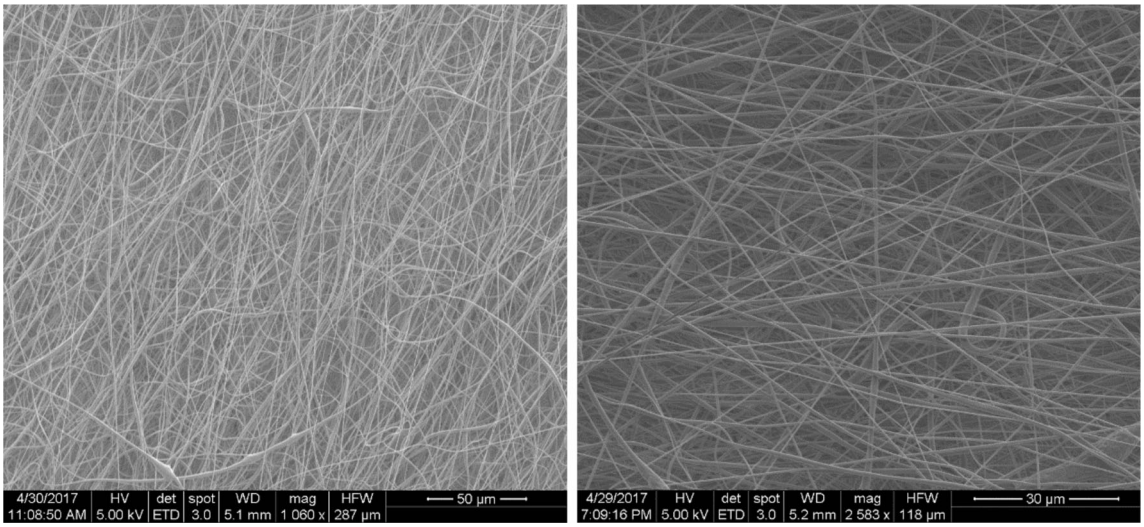

Fig. 10 The SEM images of PVDF nanofiber samples optimized by multi-objective optimization process

reduce the beta-phase content below 50%. Figure 8 shows that the fraction of beta phase can be enhanced by applying higher electrical field. The fraction of β-phase increases with increasing electrical field for all PVDF nanofiber samples. It has to be noted that this effect was more pronounced for the samples subjected at higher voltage. At high voltage, the electrospun jet is subjected to the elongation force because of an increased number of charges. In addition, a high electric field is induced between the needle and conductive drum collector at high voltage. This electrical field acts as the polling process which can further enhance the fraction of beta phase in PVDF nanofiber samples [44]. As presented in trace plot, flow rate does not show any significant effect on the beta-phase fraction.

3.4 Numerical optimization

A numerical optimization was conducted to develop a bead-free PVDF nanofiber with the maximum fraction of the beta phase. The global desirability function [45] was used to optimize any combination of one or more goals (Eq. 2):

$$D = \left(d_1^{r_1} \times d_2^{r_2} \times d_3^{r_3} \times \ldots \times d_n^{r_n}\right)^{1/\Sigma r_i} = \left[\prod_{i=1}^{n} di^{r_i}\right]^{1/\Sigma r_i} \quad (2)$$

where n is the number of responses included in the optimization and r_i is the relative importance of each individual function d_i. Importance (r_i) varies from 1 to 5, respectively from

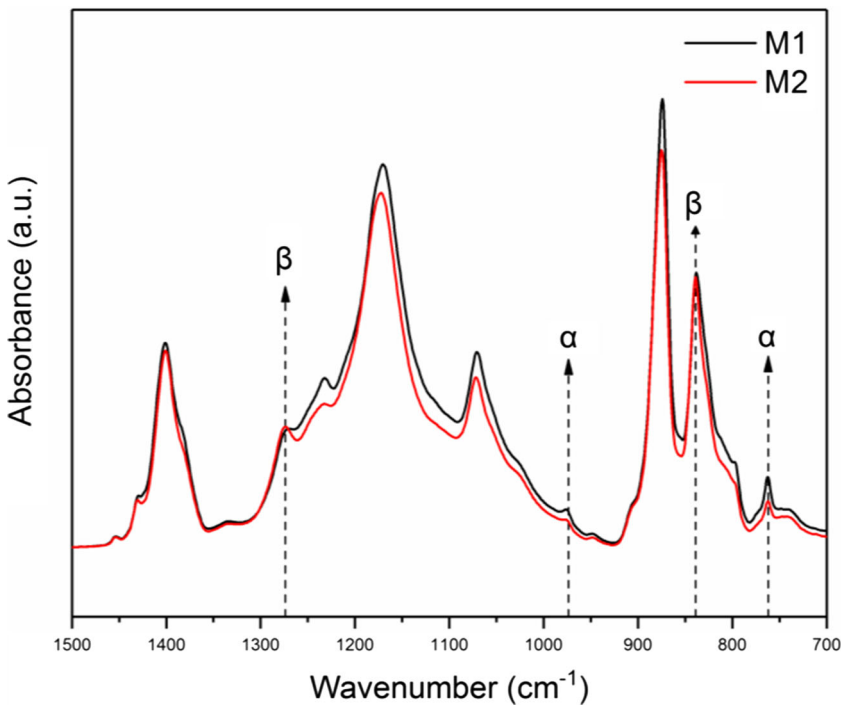

Fig. 11 The FTIR curve of PVDF nanofiber samples optimized by multi-objective optimization process

least to most important. Individual desirability functions (d_i) range between 0, for a completely undesired response, and 1, for a fully desired response. For a value of D close to 1, the combination of different criteria is globally optimal so the response values are near to the target values [28, 29].

In this study, two criteria have been defined to achieve a bead-free PVDF nanofiber with the highest fraction of beta phase. Table 3 shows all parameters and responses with their limits range, required for conducting numerical optimization. Figure 9 presents a two-response optimization zone, in which the highest beta-phase fraction and lowest number of beads were found to reach the highest desirability function. Two different optimal solutions, with the desirability of the functions ranging from 0.94 to 0.96, were obtained from the multi-objective optimization process. The predicted optimal solution and electrospinning parameters (M_1, M_2) and corresponding response values are shown in Table 4. The morphology of both optimal solution is presented in Fig. 10. The SEM picture shows the formation of beadless electrospun PVDF nanofiber for both optimal samples. The fraction of beta phase was determined by FTIR technique as shown in Fig. 11. The nanofiber sizes of M_1 and M_2 are 265 and 295 nm, respectively, which are aligned with the defined range for the optimization process. The samples exhibited 75 and 71% of fraction of beta-phase content, respectively, which satisfy the minimum criteria in the optimization process. Results confirmed that the experimental values are in good agreement with the values predicted by the proposed model.

4 Conclusions

This study proposed a robust model based on RSM method to predict the characteristics of PVDF nanofiber in terms of both morphological and fraction of beta-phase content. The model was further used to assess the effect of each individual electrospinning process parameter as well as the combined effect on the electrospun PVDF properties. A numerical optimization was conducted to achieve a beadless PVDF nanofiber with the maximum fraction of the beta phase. The RSM model was established which provides a thorough examination of PVDF nanofiber over the selected range of the electrospinning process parameters. The high values of coefficients of multiple determinations (R^2) showed the accuracy of the model to predict the characteristics of PVDF nanofiber in terms of both morphological and fraction of beta-phase content. The ANOVA results also confirmed that the inclusions of all model parameters are statistically significant based on very low P value. The higher concentration led to larger nanofiber size due to the higher solution viscosity and stronger intermolecular interactions. Also, for a constant electrical field and flow rate, the higher DMF/acetone ratio led to a finer fiber size, as higher acetone content increases the evaporation rate. The results indicated the number of beads was reduced drastically for the solution with the concentration above 25%. However, the results revealed that the high concentration solution itself does not necessarily result in a bead-free nanofiber. The increase in DMF/acetone ratio results in nanofiber characterized by more beads which might be due to the incomplete solvent evaporation. The fraction of β-phase is considerably affected by evaporation rate so that the high concentration of PVDF and DMF/acetone decreases the evaporation rate of the solution resulting in a formation of a high fraction beta-phase content. A numerical optimization was also conducted to achieve a beadless PVDF nanofiber with the maximum fraction of the beta phase. The accuracy of the obtained results was confirmed by executing a new series of experimental tests.

Funding information The authors at Purdue University are grateful to the funding supports from National Science Foundation (NSF CMMI–1560834) and Purdue Research Foundation.

References

1. Ghafari E, Witkoske E, Liu Y, Zhang C, Jiang X, Bukowski A, Kucukgok B, Lundstrom M, Ferguson IT, Lu N (2017) Waste energy harvesting using III-nitrides materials. III-Nitride materials, devices and nano-structures p 37
2. Lu N, Ferguson I (2013) III-nitrides for energy production: photovoltaic and thermoelectric applications. Semicond Sci Technol 28(7):074023
3. Feng Y, Jiang X, Ghafari E, Kucukgok B, Zhang C, Ferguson I, Lu N (2017) Metal oxides for thermoelectric power generation and beyond. Adv Composites Sci
4. Hussain B, Raja M, Lu N, Ferguson I (2013) Applications and synthesis of zinc oxide: an emerging wide bandgap material. in High Capacity Optical Networks and Enabling Technologies (HONET-CNS), 2013 10th International Conference on. IEEE
5. Tong T, Fu D, Levander AX, Schaff WJ, Pantha BN, Lu N, Liu B, Ferguson I, Zhang R, Lin JY (2013) Suppression of thermal conductivity in InxGa1− xN alloys by nanometer-scale disorder. Appl Phys Lett 102(12):121906
6. Wang Z, Song J (2006) Piezoelectric nanogenerators based on zinc oxide nanowire arrays. Science 312(5771):242–246
7. Gu L, Cui N, Cheng L, Xu Q, Bai S, Yuan M, Wu W, Liu J, Zhao Y, Ma F (2012) Flexible fiber nanogenerator with 209 V output voltage directly powers a light-emitting diode. Nano Lett 13(1):91–94
8. Zhang G, Xu S, Shi Y (2011) Electromechanical coupling of lead zirconate titanate nanofibres. IET Micro & Nano Letters 6(1):59–61
9. Sun Z, Zhang L, Dang F, Liu Y, Fei Z, Shao Q, Lin H, Guo J, Xiang L, Yerra N (2017) Experimental and simulation understanding of morphology controlled barium titanate nanoparticles under co-adsorption of surfactants. Cryst Eng Comm
10. Chang C, Tran VH, Wang J, Fuh Y-K, Lin L (2010) Direct-write piezoelectric polymeric nanogenerator with high energy conversion efficiency. Nano Lett 10(2):726–731
11. Li M, Wondergem H, Spijkman M, Asadi K, Katsouras I, Blom P, De Leeuw D (2013) Revisiting the [delta]-phase of poly (vinylidene fluoride) for solution-processed ferroelectric thin films. Nat Mater 12(5):433
12. Aqeel SM, Huanga Z, Walton J, Baker C, Falkner D, Liu Z, Wang Z (2017) Advanced functional polyvinylidene fluoride (PVDF)/polyacrilonitrile (PAN) organic semiconductor assisted by aligned

nanocarbon toward energy storage and conversion. Adv Composites Sci
13. Bodkhe S, Rajesh P, Kamle S, Verma V (2014) Beta-phase enhancement in polyvinylidene fluoride through filler addition: comparing cellulose with carbon nanotubes and clay. J Polym Res 21(5):434
14. Bassiri-Gharb N, Fujii I, Hong E, Trolier-McKinstry S, Taylor DV, Damjanovic D (2007) Domain wall contributions to the properties of piezoelectric thin films. J Electroceram 19(1):49–67
15. Liu Z, Pan CT, Lin LW, Li HW, Ke CA, Huang JC, Wang PS (2013) Mechanical properties of piezoelectric PVDF/MWCNT fibers prepared by flat/hollow cylindrical near-field electrospinning process. in Nano/Micro Engineered and Molecular Systems (NEMS), 2013 8th IEEE International Conference on. IEEE
16. Pu J, Yan X, Jiang Y, Chang C, Lin L (2010) Piezoelectric actuation of direct-write electrospun fibers. Sensors Actuators A Phys 164(1): 131–136
17. Guo H-F, Li Z-S, Dong S-W, Chen W-J, Deng L, Wang Y-F, Ying D-J (2012) Piezoelectric PU/PVDF electrospun scaffolds for wound healing applications. Colloids Surf B: Biointerfaces 96: 29–36
18. Cozza E, Monticelli O, Marsano E, Cebe P (2013) On the electrospinning of PVDF: influence of the experimental conditions on the nanofiber properties. Polym Int 62(1):41–48
19. Sencadas V, Ribeiro C, Bdikin I, Kholkin A, Lanceros-Mendez S (2012) Local piezoelectric response of single poly (vinylidene fluoride) electrospun fibers. Phys Status Solidi A 209(12):2605–2609
20. Damaraju S, Wu S, Jaffe M, Arinzeh T (2013) Structural changes in PVDF fibers due to electrospinning and its effect on biological function. Biomed Mater 8(4):045007
21. Ghafari E, Feng Y, Liu Y, Ferguson I, Lu N (2017) Investigating process-structure relations of ZnO nanofiber via electrospinning method. Compos Part B 116:40–21
22. Lei T, Yu L, Zheng G, Wang L, Wu D, Sun D (2015) Electrospinning-induced preferred dipole orientation in PVDF fibers. J Mater Sci 50(12):4342–4347
23. Baqeri M, Abolhasani M, Mozdianfard M, Guo Q, Oroumei A, Naebe M (2015) Influence of processing conditions on polymorphic behavior, crystallinity, and morphology of electrospun poly (VInylidene fluoride) nanofibers. J Appl Polym Sci 132(30)
24. Nascimento A (2014) Electrospinning of nanofiber composite from solution of poly (vinylidene fluoride)/carbon nanotube. Revista Politécnica 33(1)
25. Costa L, Bretas R, Gregorio R (2010) Effect of solution concentration on the electrospray/electrospinning transition and on the crystalline phase of PVDF. Mater Sci Appl 1(04):247
26. Montgomery DC (2005) Design and analysis of experiments: response surface method and designs. New Jersey
27. Ghafari E, Costa H, Júlio E (2013) Development of ultra high performance self compacting concrete. in Proceedings of the fifth North American conference on the SCC design and use of self-consolidating concrete. Chicago, USA
28. Ghafari E, Hugo C, Júlio E (2014) RSM-based model to predict the performance of self-compacting UHPC reinforced with hybrid steel micro-fibers. Constr Build Mater 66(0):375–383
29. Ghafari E, Costa H, Júlio E (2015) Statistical mixture design approach for eco-efficient UHPC. Cem Concr Compos 55(0):17–25
30. Alyamac K, Ghafari E, Ince R (2017) Development of eco-efficient self-compacting concrete with waste marble powder using the response surface method. J Clean Prod 144:192–202
31. Ghafari E, Bandarabadi M, Costa H, Júlio E (2012) Design of UHPC using artificial neural networks in 10th international symposium on brittle matrix composites. Warsaw, Poland
32. Ghafari E, Bandarabadi M, Costa H, Júlio E (2015) Prediction of fresh and hardened state properties of UHPC: comparative study of statistical mixture design and an artificial neural network model. J Mater Civ Eng
33. Ghafari E, Costa H, Júlio E (2014) New robust design approach for optmized sustainable UHPC. in The Fourth International fib Congress. Mumbai
34. Simon MJ, Lagergren ES, Wathne LG (1999) Optimizing high-performance concrete mixtures using statistical response surface methods. in International Symposium on Utilization of High-Strength/High-Performance Concrete. Oslo, Norway
35. Liu Y, He J-H, Yu J, Zeng H (2008) Controlling numbers and sizes of beads in electrospun nanofibers. Polym Int 57(4):632–636
36. Miyoshi T, Toyohara K, Minematsu H (2005) Preparation of ultrafine fibrous zein membranes via electrospinning. Polym Int 54(8): 1187–1190
37. Yuan X, Zhang Y, Dong C, Sheng J (2004) Morphology of ultrafine polysulfone fibers prepared by electrospinning. Polym Int 53(11): 1704–1710
38. Yarin A (1993) Free liquid jets and films: hydrodynamics and rheology. Longman Publishing Group
39. Entov V, Shmaryan LE (1997) Numerical modeling of the capillary breakup of jets of polymeric liquids. Fluid dynamics 32(5):696–703
40. Correia D, Gonçalves R, Ribeiro C, Sencadas V, Botelho G, Ribelles J, Lanceros-Méndez S (2014) Electrosprayed poly (vinylidene fluoride) microparticles for tissue engineering applications. RSC Adv 4(62):33013–33021
41. Li Z, Wang C (2013) Effects of working parameters on electrospinning, in one-dimensional nanostructures. Springer p 15–28
42. Martins P, Lopes AC, Lanceros-Mendez S (2014) Electroactive phases of poly (vinylidene fluoride): determination, processing and applications. Prog Polym Sci 39(4):683–706
43. Chinaglia D, Gregorio R, Stefanello J, Pisani Altafim R, Wirges W, Wang F, Gerhard R (2010) Influence of the solvent evaporation rate on the crystalline phases of solution-cast poly (vinylidene fluoride) films. J Appl Polym Sci 116(2):785–791
44. Andrew J, Clarke DR (2008) Effect of electrospinning on the ferroelectric phase content of polyvinylidene difluoride fibers. Langmuir 24(3):670–672
45. Derringer GC, Suich R (1980) Simultaneous optimization of several response variables. J Qual Technol 12(4):214–219